THE JOURNAL OF PHYSICAL CHEMISTRY C

Article

pubs.acs.org/JPCC

Mechanistic Studies of Formate Oxidation on Platinum in Alkaline Medium

Jimmy John, Hongsen Wang, Eric D. Rus, and Héctor D. Abruña*

Department of Chemistry and Chemical Biology, Baker Laboratory, Cornell University, Ithaca, New York 14853-1301, United States

ABSTRACT: The electro-oxidation of formate ($HCOO^-$) on polycrystalline Pt in highly basic medium (pH = 14) has been investigated by cyclic voltammetry, differential electrochemical mass spectrometry, potential step-linear sweep voltammetry, and adsorbate stripping experiments. Low oxidation currents were observed for $HCOO^-$ oxidation indicating that $HCOO^-$ is only weakly active under these conditions. The activity of $HCOO^-$ is confined to low potentials (0.2 V < E < 0.7 V vs RHE). Our results suggest a dual pathway mechanism for $HCOO^-$ oxidation, analogous to HCOOH oxidation in acid. In the case of $HCOO^-$ oxidation, the direct and indirect pathway analogues are referred to as the primary and secondary pathways, respectively. Formation of CO_{ads} from $HCOO^-$ was observed to be slow. We also find that oxidation of CO_{ads} (the secondary pathway) is strongly coupled to the oxidation of $HCOO^-$ through the primary pathway. Moreover, the oxidation of CO_{ads} did not appreciably enhance $HCOO^-$ oxidation through the primary pathway, signifying the presence of other inhibitory processes such as OH adsorption. Adsorbate stripping experiments revealed, in addition to CO_{ads}, the presence of a stable adsorbate that can undergo oxidation. We also find that the latter can be converted to CO_{ads} in the H_{upd} region. On the basis of the results obtained, a tentative mechanism of $HCOO^-$ oxidation in basic media is proposed.

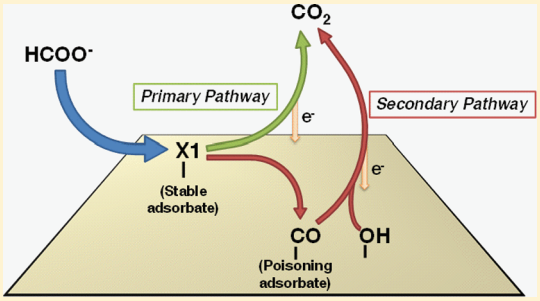

1. INTRODUCTION

HCOOH oxidation on platinum in acidic conditions has been a topic of extensive research for over four decades.[1−14] Its oxidation is generally accepted to proceed via the dual-pathway mechanism.[3,9,13] This is shown in Scheme 1 (based on the mechanism proposed by Sun et al.[9]). HCOOH can undergo rapid and direct oxidation to CO_2 via the so-called direct pathway. The reactive intermediate in this pathway is believed to be [Pt]-COOH.[3,9,13] Alternatively, HCOOH can decompose to the poisoning species, adsorbed CO (CO_{ads}), which can be subsequently oxidized to CO_2 at higher potentials.[9] However, there has been only a handful of studies of $HCOO^-$ oxidation on Pt (vide infra). In the interest of clarity, we define $HCOO^-$ oxidation as the bulk oxidation of $HCOO^-$ under conditions of negligible concentration of HCOOH in solution. Given that the pK_a of HCOOH ≈ 3.8, this necessarily implies that the oxidation of $HCOO^-$ occurs at solution pHs well above the pK_a of HCOOH (i.e., neutral and basic pHs).

Scheme 1. Mechanism of HCOOH Oxidation in Acid (Based on Ref 9)

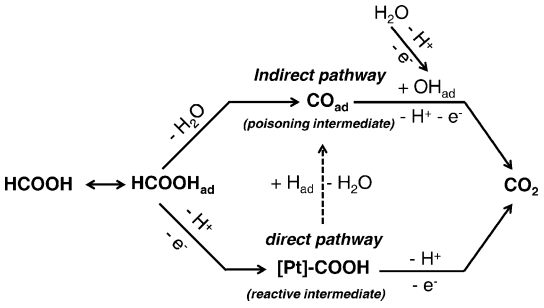

As one of the simplest electrocatalytic reactions, HCOOH oxidation on Pt is of importance as a model reaction in fundamental electrocatalysis. Hence, elucidating the oxidative mechanism of $HCOO^-$ would extend our understanding of the oxidation of the HCOOH/$HCOO^-$ system over the entire range of pH (0−14). Moreover, even in the extensively studied case of HCOOH oxidation in acid on Pt, recent in situ FTIR studies have led to the proposal of a third pathway involving adsorbed formate ($HCOO_{ads}$).[15−19] Technologically, the recent advent of alkaline anion exchange membranes (AAEMs) has resulted in renewed interest in alkaline fuel cells.[20,21] This development warrants a reinvestigation of the electrocatalytic oxidation of small organic molecules (SOMs), $HCOO^-$ being ostensibly the simplest, under alkaline conditions. It is already known that there is a remarkable enhancement of methanol oxidation on Pt in alkaline medium.[22−26] In light of this, the study of $HCOO^-$ oxidation becomes important since it has been recently suggested that $HCOO^-$ is an important intermediate in methanol oxidation under these conditions.[27]

To the best of our knowledge, the earliest report of $HCOO^-$ oxidation on Pt was by Buck and Griffith.[28] They observed low oxidation currents at very basic pHs (12−14) compared to acidic and neutral pHs. Conway and Dzieciuch, performing a comparative study of decarboxylation reactions of trifluoroace-

Received: December 9, 2011
Published: January 16, 2012

   dx.doi.org/10.1021/jp211887x | J. Phys. Chem. C 2012, 116, 5810−5820

tate and formate in aqueous (alkaline) and nonaqueous media, found the reactions to be more complex in aqueous medium.[29] Wetzel et al. investigated $HCOO^-$ oxidation on Pt in the pH region of 10 to 13.5.[30,31] They also observed low currents but reported an abrupt enhancement of the oxidation rate when the solution pH fell below ~12.6. Beden et al.[32] and Adzic et al.[33] saw particularly high activity of Pt for $HCOO^-$ oxidation in neutral medium vis-à-vis HCOOH in acidic medium. Recently, Christensen et al.[34] reported on an in situ FTIR study of $HCOO^-$ oxidation on Pt in alkaline solution with emphasis on the role of $HCOO^-$ as an intermediate in methanol oxidation under similar basic conditions. They were able to detect formation of adsorbed CO (CO_{ads}), both linear-bonded (CO_L) and bridge-bonded (CO_B), from adsorbed formate ($HCOO_{ads}$). Nevertheless, mechanistic details of $HCOO^-$ oxidation are still very much lacking.

In the present manuscript, we report our findings of $HCOO^-$ oxidation on polycrystalline Pt under alkaline conditions. Cyclic voltammetric and differential electrochemical mass spectrometric (DEMS) techniques were employed in elucidating mechanistic details and monitoring product formation (namely CO_2). DEMS is particularly useful since it is sensitive to only volatile reaction products (see ref. 35 for a review of the technique). In the case of $HCOO^-$ oxidation, since the one and only oxidation product is the volatile CO_2, DEMS allows us to separate out and monitor just those oxidative processes generating CO_2 from overlapping processes like the Pt-surface features (H-upd, Pt-oxide formation/reduction), double layer charging, etc. This greatly simplifies the analysis of cyclic voltammograms. Since it is known that $HCOO^-$ adsorbs strongly on Pt under both acidic[15,17−19,36] and alkaline conditions,[27,34,37] we anticipated that $HCOO^-$ oxidation would be highly adsorbate mediated. To this end, adsorbate stripping experiments, using a thin layer flow cell, were conducted. These experiments are particularly useful in separating the adsorbate and the solution contributions to the overall activity. Analogous experiments in acid were also performed or literature cited, where required, to delineate the differences in $HCOO^-$ oxidation under alkaline conditions and HCOOH oxidation under acidic conditions. Finally, a tentative mechanism for $HCOO^-$ oxidation on Pt is proposed.

2. EXPERIMENTAL SECTION

2.1. Reagents. Solutions were prepared with high purity deionized water (18 MΩ cm Millipore Milli-Q). HCOONa (≥99.0% ACS Sigma Aldrich) and HCOOH (88% AR ACS Mallinckrodt) were used to make the analyte solutions. For preparing supporting electrolyte of desired pH, NaOH (99% AR ACS Mallinckrodt), H_2SO_4 (99.999% Aldrich) and $HClO_4$ (70% ACS Reagent Fisher Scientific) were used. In some experiments, a constant ionic strength was maintained by the addition of $NaClO_4$ (anhydrous 98.0−102.0% ACS Alfa Aesar) to the solution.

2.2. Electrochemical Measurements. Cyclic voltammetric studies were carried out in a conventional three-electrode electrochemical cell. For adsorbate stripping experiments, a homemade dual thin-layer flow cell was employed. Construction of this cell has been described in detail elsewhere.[38,39] To accomplish the fast exchange between analyte and supporting electrolyte (blank) solutions while maintaining potential control, a three way luer valve was used to switch between reservoirs of blank and analyte solutions. For both cyclic voltammetric and adsorbate stripping experiments, polycrystalline Pt disks (5 or 10 mm in diameter) were used as the working electrode. In case of the thin layer flow cell, used for adsorbate stripping experiments, a circular area, 6 mm in diameter, of the Pt disk is exposed to the solution.

Due to the rapid conversion of CO_2 to CO_3^{2-} in alkaline conditions, mass spectrometric detection of CO_2 was not possible with the aforementioned dual thin-layer flow cell used for adsorbate stripping experiments. For DEMS experiments, a homemade conventional type cell was employed. Details of such a cell have been described elsewhere.[40] Briefly, the cell body is fabricated out of chemically resistant KEL-F. Pt, sputtered to an average thickness of ~30 nm on a porous Teflon membrane (GORE-TEX), was used as the working electrode. The working electrode was mechanically supported on a porous stainless steel frit which was interfaced to the vacuum system of the mass spectrometer. Since CO_2 generation in such a configuration occurs right on the porous membrane, a short delay time of the mass spectrometric signal is achieved. It is to be noted that the solution is stationary inside the DEMS cell.

Measurements were made using an EG&G Model 173 potentiostat/galvanostat and Model 175 universal programmer. For some experiments, a Pine AFCBP1 Bipotentiostat, a PAR Model M-273 potentiostat or a BASi CV-27 voltammograph was also used. Data were recorded through a homemade data acquisition software (CV-EI400) using a NI-DAQ card. All solutions were deaerated with high purity argon (Airgas) for at least 30 min prior to the experiment. Measurements were carried out at room temperature. A large area Pt wire was used as the counter electrode and a RHE as the reference electrode. All potentials are referenced to RHE. Where current densities (j) are reported, the currents (i) are always normalized to the geometric surface area of the working electrode.

2.3. DEMS Apparatus. The mass spectrometer system and associated components, used for DEMS studies, have been previously described.[41] A primsa plus mass spectrometer system, along with the vacuum system components were obtained from Pfeiffer vacuum. Quadera software (supplied by Pfeiffer vacuum) was used to control the mass spectrometer. A cross beam ion source, with a nominal electron impact energy of 65 eV was used for ionization and a Faraday cup was used for ion detection. The analog output signals from the mass spectrometer were acquired using a NI-DAQ card and recorded by a homemade LabVIEW program which also simultaneously recorded data from the concomitant electrochemical measurements.

2.4. Electrode Preparation. Prior to each experiment, where polycrystalline Pt disks were used, the working electrodes were polished with 1 μm diamond paste (METADI Buehler) to a mirror finish, rinsed with ultrapure water, and sonicated in ultrapure water three times, each time for 10 min. Pt wire counter electrodes were also flame annealed in a propane flame to ensure cleanliness. For all working electrodes, electrochemical cycling over the potential window from 0.05 to 1.4 V vs RHE at 100 mV/s was also carried out in respective supporting electrolyte until clean Pt cyclic voltammograms were obtained. When comparable experiments were carried out in acid and in base, the same experimental conditions were maintained including using the same electrochemical cell, working electrode, reference electrode (RHE), and counter electrode; except, of course, the analyte and the supporting electrolyte solutions.

dx.doi.org/10.1021/jp211887x | J. Phys. Chem. C 2012, 116, 5810−5820

3. RESULTS

3.1. Cyclic Voltammetric Studies. Representative cyclic voltammograms of HCOOH oxidation in acid and $HCOO^-$ oxidation in base on Pt are shown in Figure 1a,b, respectively.

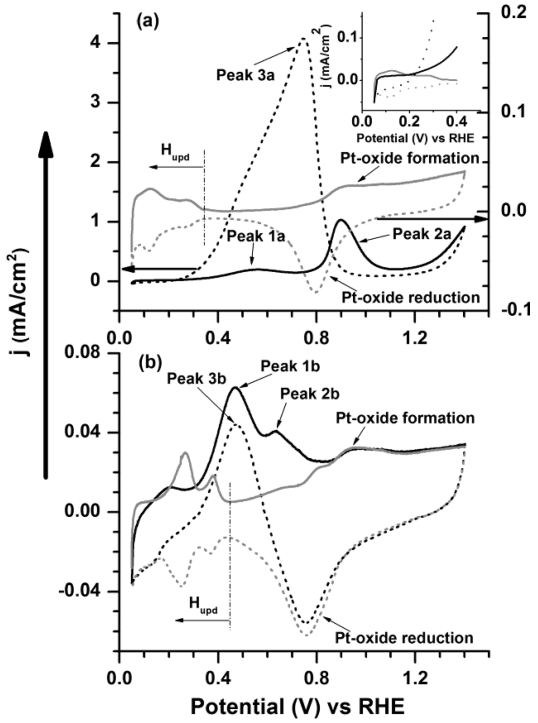

Figure 1. Cyclic voltammograms of (a) 0.2 M HCOOH in 1 M $HClO_4$ (Black) on a polycrystalline Pt disk and (b) 0.2 M HCOONa in 1 M NaOH (Black). Cyclic voltammograms of blank solutions (1 M $HClO_4$ and 1 M NaOH, respectively) are shown in gray. Inset to Figure 1a shows the H_{upd} region in 1 M $HClO_4$ (Gray) and in the presence of 200 mM HCOOH (Black). Positive-going and negative-going segments of the cyclic voltammograms are shown by solid lines and broken lines, respectively. Scan rate 20 mV/s.

Since the voltammetric features (Figure 1a) of HCOOH oxidation are relatively well understood,[1−13] it is worthwhile to review the same for the sake of comparing them to those of $HCOO^-$ oxidation. In the positive−going scan, the onset of oxidation occurs at about ∼0.2 V (see inset to Figure 1a, also refs 9, 42), and displays two peaks: (i) a small peak at ∼0.56 V (**Peak 1a**) corresponding to the direct oxidation of HCOOH at Pt sites not blocked by CO_{ads}, and (ii) a larger peak at ∼0.9 V (**Peak 2a**) that has contributions from both the indirect (oxidation of CO_{ads}, see Scheme 1) and the direct pathways. The latter contribution is enhanced due to the removal of site-blocking CO_{ads} by electro-oxidation. HCOOH can also be oxidized in the Pt-oxide region. The onset of this oxidative process is seen at ∼1.2 V. This is thought to be due to the presence of catalytically active surface oxides that can oxidize HCOOH, presumably through an Eley−Rideal mechanism.[13,28,43] In the negative-going scan, much higher currents are observed as a result of facile electro-oxidation of HCOOH on CO_{ads} free Pt surface. The onset of the oxidation peak (**Peak 3a**) in the negative-going scan is ∼0.9 V.

Since Pt-surface processes, especially H and OH adsorption, can potentially influence the oxidation of $HCOO^-$ in alkaline media, we also summarize here our current understanding of H and OH adsorption processes on Pt in alkaline medium vis-à-vis acidic medium.[44−46] In acid on Pt, H-adsorption/desorption and OH/O formation/reduction processes are well-separated in potential ranges, i.e., the processes are decoupled. However, in alkaline medium, these processes are not necessarily separated; specifically, coupled H and OH adsorption/desorption processes are thought to occur reversibly up to ∼0.65 V vs RHE on Pt (100) and Pt (110) faces. The onset of OH adsorption on Pt in alkaline medium is quite early at ∼0.35 V vs RHE.[46,47] An important consequence of this availability of OH_{ads} at low potentials is the significantly lower onset potential for CO_{ads} oxidation on Pt in alkaline medium[48−52]compared to acidic medium. Additional details can be found in the aforementioned references.

While comparing the activities of HCOOH and $HCOO^-$ for oxidation (Figure 1), it is observed that the oxidative currents during $HCOO^-$ oxidation are significantly lower than those of HCOOH oxidation (∼90× lower on comparing the peak currents for **Peak 3a,b** in the negative-going scans) for the same bulk concentration of $HCOO^-$ and HCOOH. This indicates that $HCOO^-$ oxidation is kinetically much slower than HCOOH oxidation. For $HCOO^-$ oxidation, two peaks (**Peak 1b** and **Peak 2b**) are observed in the positive-going scan and one peak (**Peak 3b**) in the negative-going scan (Figure 1b). The first peak (**Peak 1b**) in the positive-going scan and the peak (**Peak 3b**) in the negative-going scan occur at about the same potential (∼0.47 V) and also have comparable peak currents. The second peak (**Peak 2b**) in the positive-going scan at ∼0.63 V is smaller than the first peak (**Peak 1b**). The mass spectrometric cyclic voltammogram (MSCV) of CO_2 (Figure 2b) at m/z = 44 (CO_2^+) recorded simultaneously with the

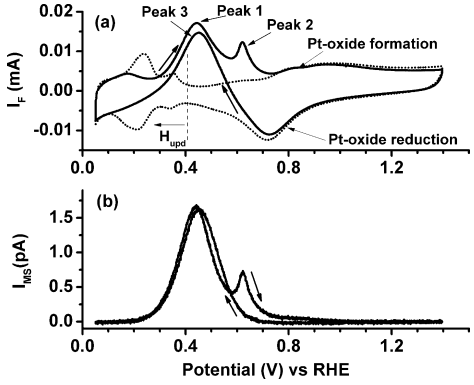

Figure 2. Simultaneously recorded (a) cylic voltammogram and (b) corresponding mass spectrometric cyclic voltammogram at m/z = 44 (CO_2^+) for $HCOO^-$ oxidation on a Pt sputtered Teflon membrane in 0.1 M HCOONa + 1 M NaOH. Cyclic voltammogram of 1 M NaOH shown in dotted line in part a. Scan rate: 10 mV/s.

electrochemical measurement (Figure 2a) serves to conveniently monitor product formation during $HCOO^-$ oxidation, namely CO_2. From the onset of the mass spectrometric current, it is clear that the onset of $HCOO^-$ oxidation is ∼0.2 V. No CO_2 is detected in the negative-going scan above ∼0.7 V. It is apparent that $HCOO^-$ oxidation is completely suppressed in the Pt-oxide region. On the basis of these results, we conclude that $HCOO^-$ oxidation only occurs over a limited potential range approximately from 0.2 to 0.7 V.

It has been suggested that the dual pathway mechanism, active for HCOOH oxidation (Scheme 1), is generally applicable for $HCOO^-$ oxidation.[1] In essence, analogous to HCOOH, it has been proposed that $HCOO^-$ can undergo

dx.doi.org/10.1021/jp211887x | J. Phys. Chem. C 2012, 116, 5810−5820

oxidation either directly through a reactive intermediate or indirectly through a chemisorbed or poisoning intermediate. The presence of a chemisorbed intermediate has been verified and identified as CO_{ads} by the recent in situ FTIR study by Christensen et al.[34] The presence of the site-blocking CO_{ads} species is also apparent from the diminution of both the broad H-desorption peak (~0.2 V) in the positive-going scan and the H-adsorption peaks in the range 0.05−0.3 V in the negative-going scan in Figure 1b. The identity of the reactive intermediate, if present, is not known yet. It has been suggested that there are slow prechemical steps such as adsorption and/or formation of the reactive intermediate that could be rate-limiting.[28,53] Consequently, it has been proposed that the low activity of $HCOO^-$ can be attributed to such limiting processes in alkaline solution.[1,53] With this literature premise, we seek to understand the voltammetric features of $HCOO^-$ oxidation.

Separation and identification of Faradaic processes associated with $HCOO^-$ oxidation is problematic due to the significant overlap between processes. For instance, referring to Figure 2, it is clear that the potential ranges of the Faradaic processes underlying the two peaks (**Peak 1** and **Peak 2**) in the positive-going scan overlap considerably. Given that CO_{ads} formed from $HCOO^-$ has already been detected[34] and that the oxidation of bulk and adsorbed CO has already been observed at potentials at which **Peak 2** occurs,[52] we can conclude that **Peak 2** has contributions from the oxidation of CO_{ads}. Due to similar peak positions and onset potentials, the oxidative process underlying **Peak 1** in the positive-going scan and **Peak 3** in the negative-going scan is inferred to be the same. As concluded earlier based on the DEMS results (Figure 2b), this Faradaic process is active over a potential range approximately from 0.2 to 0.7 V. One possibility is the oxidation of CO_{ads}. It is well-known that, on Pt, CO_{ads} can be oxidized at significantly more negative potentials (as low as 0.35 V[51]) in base than in acid.[48−52] Hence, we should expect a contribution from CO_{ads} oxidation to **Peak 1**. However, CO_{ads} oxidation cannot account for the quite negative onset (~0.2 V) of $HCOO^-$ oxidation at which potential no OH-adsorption is expected to occur.[46,47] This is also supported by the findings from the in situ FTIR study of $HCOO^-$ oxidation by Christensen et al.[34] where they observed CO_3^{2-} formation at a potential lower than the onset of OH-adsorption. Thus, it is inferred that this process involves the oxidation of $HCOO^-$ by another pathway not involving CO_{ads}. Hence, our results also support, in essence, the dual pathway mechanism of $HCOO^-$ oxidation. In summary, it appears that **Peak 2** is mainly the oxidation of CO_{ads}, analogous to the indirect pathway of HCOOH oxidation. **Peak 1** corresponds mainly to an oxidative pathway not involving CO_{ads}. Since it is not certain that $HCOO^-$ is directly converted to CO_2 in this pathway, we prefer to call this oxidative process the *primary pathway*. Relatedly, in the context of $HCOO^-$ oxidation, we refer to the conventional indirect pathway through CO_{ads} oxidation as the *secondary pathway*.

On comparing CVs of $HCOO^-$ and HCOOH oxidation, we find notable differences (see Figure 1). In the case of HCOOH oxidation (Figure 1a), it is generally observed that the removal of the site-blocking CO_{ads} by electro-oxidation results in a significant enhancement of HCOOH oxidation. This is seen from the higher currents for the second peak (**Peak 2a**) compared to the first peak (**Peak 1a**) in the positive-going scan and also from the siginificantly higher currents during the negative-going scan. Analogously, in the case of $HCOO^-$ oxidation, if CO_{ads} were highly inhibitory, then we should expect improvement in $HCOO^-$ oxidation upon removal of CO_{ads}. However, as noted earlier, low currents are observed in both the positive and the negative-going scans for $HCOO^-$ oxidation. In fact, from Figure 1b it is seen that the peak currents are comparable in the positive and the negative-going scans. We also note that that the second peak (**Peak 2b**) is smaller than the first (**Peak 1b**) in the positive-going scan. From these observations, it can be concluded that the surface blocking by CO_{ads} formation from $HCOO^-$ is not the primary reason for the apparent low activity of $HCOO^-$.

$HCOO^-$ oxidation is completely inhibited in the Pt-oxide region (see Figures 1 and 2). This is in contrast to HCOOH in acid where Pt-oxide is catalytically active toward oxidation of HCOOH.[13,28,43] It may be that the Pt-oxide formed in alkaline solution is unreactive toward $HCOO^-$. It is also important to consider the charged nature of $HCOO^-$. In the Pt-oxide region, at potentials well positive of PZC,[54−56] it is possible that $HCOO^-$ behaves just as a spectator anion at the surface. Significantly, Vela et al.,[57] studying HCOOH and HCOONa oxidation at Pd in acid and alkaline solutions by in situ FTIR spectroscopy, showed the presence of a predominant surface configuration of $HCOO^-$ in alkaline solution with the two O-atoms bound strongly to the Pd surface and the C−H bond normal to the surface. Employing surface enhanced infrared absorption (SEIRA) spectroscopy, a surface-sensitive in situ FTIR technique, to study HCOOH oxidation in acid at Pt nanoparticles, Miki et al. show that $HCOO_{ads}$ is most likely to be in a bridging configuration on the Pt-surface with the molecular plane normal to the surface or slightly tilted.[58] On the basis of the computational results, similar conclusions were reached by Neurock et al.[59] in the context of the role of $HCOO^-$ in HCOOH oxidation at Pt in acid. The salient point of such studies is that the C−H bond activation in such a surface configuration would be difficult, consistent with the observed lack of activity for $HCOO^-$ oxidation in the Pt-oxide region. It is also interesting to note that $HCOO^-$ oxidation in the cathodic scan is initiated only after significant Pt-oxide reduction (see Figure 2). However, the onset of HCOOH oxidation coincides with the onset of the Pt-oxide reduction peak (see Figure 1a).

To further understand the low activity of $HCOO^-$, the bulk concentration of $HCOO^-$ was varied while keeping $[OH^-]$ the same and the ionic strength constant at 1.2 M (Figure 3a). The latter was achieved by the addition of appropriate amounts of $NaClO_4$ to the different analyte solutions. Examination of the anodic scans shows several trends in the voltammetric response (Figure 3b). First, there is an increase of the first (**Peak 1**) and the second (**Peak 2**) peak currents in the positive-gong scan with $[HCOO^-]$. Since we expect $HCOO^-$ oxidation to be adsorbate mediated, it could be that there is an increase in the surface concentration of an active intermediate with $[HCOO^-]$, dictated by an appropriate isotherm. Second, although both **Peak 1** and **Peak 2** increase, **Peak 1** increases faster than **Peak 2** with increasing $[HCOO^-]$, i.e., the direct oxidation of $HCOO^-$ occurs to a greater extent than the oxidation of CO_{ads} at higher concentrations of $HCOO^-$. It is possible and likely that at high concentrations of $HCOO^-$, CO_{ads} formed from $HCOO^-$ approaches a saturation coverage. Hence, the incremental increase in the charge of CO_{ads} oxidation would be less at higher $[HCOO^-]$. Third, there is a progressive increase in the suppression of the H-desorption peak (~0.2 V) with $[HCOO^-]$ possibly from increased CO_{ads} formation. The peak (**Peak 3**) in the negative-going scan (inset to Figure 3a),

dx.doi.org/10.1021/jp211887x | J. Phys. Chem. C 2012, 116, 5810−5820

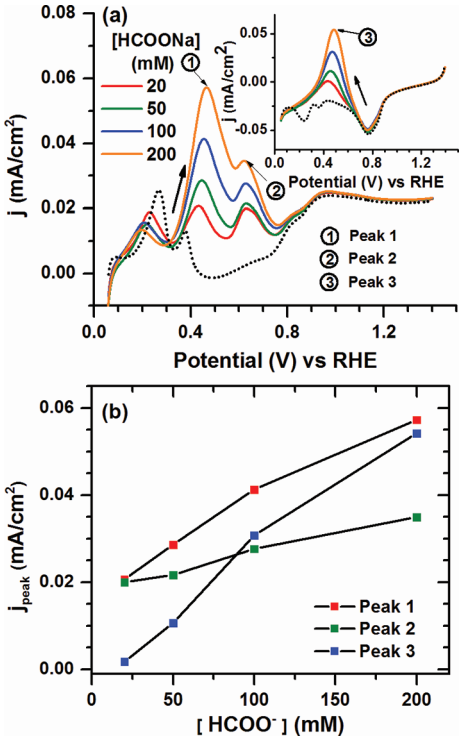

Figure 3. (a) Positive-going segments of cyclic voltammograms at different concentrations of HCOONa in 1 M NaOH with appropriate amounts of $NaClO_4$ added to keep the ionic strength constant at 1.2 M on a polycrystalline Pt disk. Inset shows the corresponding negative-going segments. Positive and negative-going segments of the cyclic voltammogram of 1 M NaOH + 0.2 M $NaClO_4$ are shown in dotted line. Scan rate 10 mV/s. (b) Peak currents (j_{peak}) of the oxidation peaks in the positive and the negative-going scans plotted versus [$HCOO^-$].

although smaller than **Peak 1**, also increases in magnitude with [$HCOO^-$]. It was previously noted (Figure 2) that the currents associated with **Peak 1** and **Peak 3** are comparable. Comparing the peak currents (Figure 3), we note that with decreasing [$HCOO^-$], **Peak 3** becomes smaller relative to **Peak 1**. This may be due to an increase in the inhibitory effects of OH adsorption at lower [$HCOO^-$] (vide infra).

The effect of change in scan rate (ν) on $HCOO^-$ oxidation is shown in Figure 4. Since the oxidation currents (Figure 4a) are

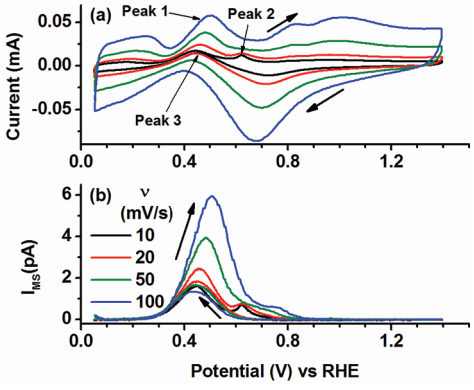

Figure 4. Simultaneously recorded (a) cyclic voltammograms and (b) corresponding mass spectrometric cyclic voltammograms at m/z = 44 (CO_2^+) on a Pt sputtered Teflon membrane in 0.1 M HCOONa + 1 M NaOH at different scan rates.

comparable to those from Pt-surface features, simultaneous MSCVs (Figure 4b) were recorded to separate out, in effect, the $HCOO^-$ oxidation currents. The mass spectrometric currents (I_{MS}) were then used to investigate the variation of $HCOO^-$ oxidation peaks with ν. However, this method is limited to relatively low scan rates due to the limit imposed by the time response of the DEMS setup.

Of significance is the behavior of **Peak 1** in the positive-going scan and **Peak 3** in the negative-going scan with ν. **Peak 1** increases with increasing ν (Figure 4a). This is clearly seen in the corresponding mass spectrometric cyclic voltammograms of CO_2 at m/z = 44 (Figure 4b). This is attributed to the time-dependent formation of the poisoning CO_{ads}. The longer the potential of the working electrode is held in the H_{upd} region, the larger the amount of CO_{ads} is formed. Thus, as the scan rate is increased, the amount of CO_{ads} formed decreases due to the decrease in the time required to traverse the H_{upd} region. Consequently, $HCOO^-$ oxidation is enhanced at higher scan rates due to decreased surface blocking by CO_{ads}. Such an effect is also observed in the case of HCOOH oxidation.[3,60,61] The former explanation is also consistent with the observation that only at low scan rates do we see a well-defined second peak, **Peak 2** (attributed mainly to CO_{ads} oxidation), in the positive-going scan. Interestingly, based on the mass spectrometric currents, $HCOO^-$ oxidation currents in the negative-going scans do not vary significantly with ν and are also smaller than that in the positive going scan (Figure 4b). In fact, the negative-going scans in the MSCVs for different values of ν overlap to a large extent. This is most likely due to OH adsorption. We explain this effect as follows. As was mentioned earlier, OH adsorption occurs at all potentials beyond ~0.35 V. It is reasonable to assume that $HCOO^-$ is unlikely to displace the OH_{ads} already present. Thus, due to a lack of adsorption sites, $HCOO^-$ oxidation is inhibited in the negative-going scan. Consequently, the $HCOO^-$ oxidation current in the negative-going scan would be smaller and independent of ν. At the start of the positive-going scan (0.05 V vs RHE), however, no OH_{ads} is present. As the positive-going scan progresses, $HCOO^-$ in solution can better compete with OH^- for adsorption sites. This could explain the scan rate dependence of **Peak 1** in the positive-going scan and also the higher oxidation currents in the positive-going scan. It is noteworthy that, under similar basic conditions, CH_3OH which exhibits high activity on Pt also shows lower currents in the negative-going scan than in the positive-going scan.[25,62]

Interestingly, Buck and Griffith[28] observed an increase in peak currents of $HCOO^-$ oxidation on decreasing the bulk pH from 14 to 10. This supports the idea of inhibition of $HCOO^-$ oxidation by OH adsorption. However, it is inherently difficult to isolate the effects of OH adsorption from adventitious processes. At lower pHs, due to the necessary requirement of a buffer system, we have to consider the effect of adsorption of counterions other than OH^-. Moreover, even in a buffered system, the pH at the electrode surface can be sensitive to small changes in bulk pH.[30] As shown by Wetzel et al.,[31] this becomes important for $HCOO^-$ oxidation since changes in surface pH could significantly change the relative concentrations of $HCOO^-$ and HCOOH near the electrode from their bulk solution values. In any case, it is clear that the effects of OH adsorption on $HCOO^-$ oxidation warrant careful study.

It is known that decomposition of HCOOH in acid to CO_{ads} (Scheme 1) can take place in two ways.[9,63] The first is the slow formation of CO_{ads} over a wide potential range (0.05 to 1.0 V)

dx.doi.org/10.1021/jp211887x | J. Phys. Chem. C 2012, 116, 5810–5820

from the spontaneous dissociative adsorption of HCOOH. Another is the rapid dehydration of HCOOH in the H_{upd} region. It is suspected that H_{ads} enhances the formation of CO_{ads} in this potential region.[3,9,14] It has been proposed that the latter method of CO_{ads} formation involves reduction of either the reactive intermediate Pt-COOH[3,9] or $HCOOH_{ads}$[14] by H_{ads}. The effect of H_{ads} on formation of CO_{ads} from HCOOH was studied by Capon and Parsons[3] by reversal of negative-going sweeps at different potentials ($\mathbf{E_{low}}$) in and near the H_{upd} region. We followed the same strategy to examine the analogous effect on formation of CO_{ads} from $HCOO^-$ and consequently on the primary and the secondary pathways of $HCOO^-$ oxidation. The results of such an experiment for HCOOH and $HCOO^-$ are shown in Figure 5a,b, respectively.

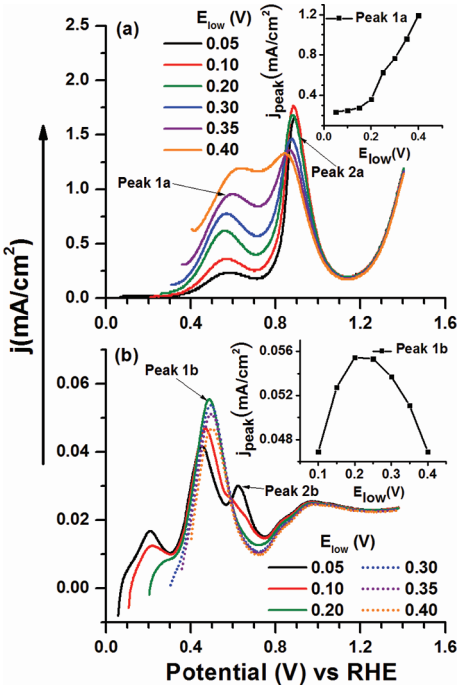

Figure 5. Positive-going segments of potential sweeps with different values for the lower limit of potential sweep (E_{low}) (a) 0.1 M HCOOH in 1 M $HClO_4$ (b) 0.1 M HCOONa in 0.9 M NaOH. Scan rate 10 mV/s. Insets to Figure 5a,b shows plots of peak currents for peaks **Peak 1a** and **Peak 1b**, respectively, in the positive-going segment (j_{peak}) versus E_{low}.

The results for HCOOH agree with those reported by Capon and Parsons.[3] As the negative limit (E_{low}) of the potential sweeps is shifted positive, there is an enhancement of the direct oxidation pathway. This is apparent from the increase in the peak current (j_{peak}) of the first peak (**Peak 1a**) in the positive-going scan with increasing E_{low} (inset to Figure 5a). This is clearly due to a decrease in the formation of site-blocking CO_{ads} with increasing E_{low}. The second peak (**Peak 2a**) in the positive-going scan decreases to a small extent due to the decrease in CO_{ads} formation with E_{low}.

Similarly, in the case of $HCOO^-$, the amount of CO_{ads} decreases with increasing E_{low}. This is evident from the decrease in the second peak (**Peak 2b**) in the positive-going scan (Figure 5b). It is possible that CO_{ads} formation from $HCOO^-$ also involves H_{ads} just as in HCOOH. However, under the conditions of potential cycling employed, **Peak 2b** in the positive-going scan is not discernible when E_{low} is above 0.2 V. This could mean that, unlike the case of HCOOH, CO_{ads} formation from $HCOO^-$is restricted to low potentials in the H_{upd} region. The behavior of **Peak 1b** in the positive-going scan in the case of $HCOO^-$ oxidation is very revealing. Instead of a monotonically increasing peak, the first peak in the positive-going scan changes anomalously with E_{low}. It grows initially, reaching a maximum at $E_{low} \approx 0.2$ V and then decreases. This is also shown more clearly in the plot of the peak current (j_{peak}) with E_{low} (inset to Figure 5b). Such a behavior may be the combined effect of inhibition of $HCOO^-$ adsorption by H and OH adsorption processes. At quite low potentials ($E_{low} \approx 0.05$ V) in the H_{upd} region, H_{ads} can prevent adsorption of $HCOO^-$. With increasing potential, however, more sites would be available for $HCOO^-$ to adsorb and undergo oxidation. Consequently, an increase in $HCOO^-$ oxidation is seen. However, at more positive potentials, $HCOO^-$ will have to compete with OH^- for adsorption sites; thus, $HCOO^-$ oxidation is again inhibited.

3.2. Potential Step-Linear Sweep Voltammetric Studies. The amount of CO_{ads} formed from HCOOH in the H_{upd} region, under potentiodynamic conditions, has been shown to be a function of both potential[63] and time.[3] We have studied similar potential and time effects for CO_{ads} formation from $HCOO^-$ using potential step-scan experiments.

For the time-dependent study of CO_{ads} formation, the potential program employed was as follows (see inset to Figure 6a). The potential of the working electrode was held initially

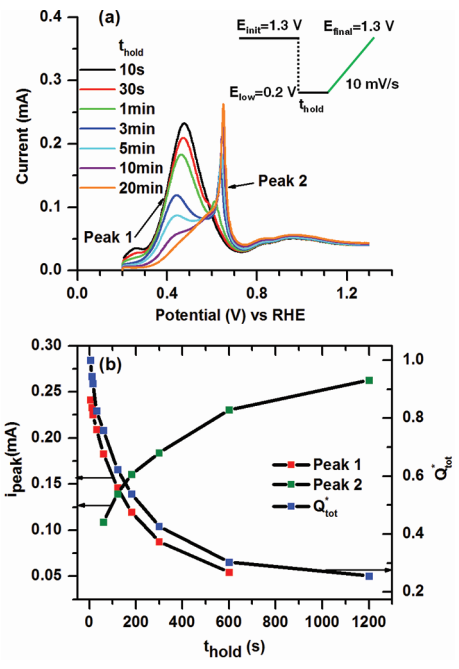

Figure 6. (a) Positive-going scans obtained after a potential step from 1.3 to 0.2 V vs RHE and held for time t_{hold} at 0.2 V on Pt sputtered Teflon membrane in 0.1 M HCOONa + 1 M NaOH. Scan rate 10 mV/s. Inset shows the potential program followed. (b) Plots of the normalized charge of $HCOO^-$ oxidation, Q_{tot}* and also the peak currents versus t_{hold}.

(E_{init}) at 1.3 V (where there is no oxidation of $HCOO^-$) in 100 mM HCOONa + 1 M NaOH. The potential was then stepped to E_{low} = 0.20 V and held for varying amounts of time (t_{hold}). This potential was chosen to minimize effects from both H and OH adsorption as it was already indicated that $HCOO^-$

dx.doi.org/10.1021/jp211887x | J. Phys. Chem. C 2012, 116, 5810–5820

adsorption may be inhibited by the former processes. After time t_{hold}, the potential was scanned, at 10 mV/s, from E_{low} = 0.20 V to E_{final} = 1.3 V. The positive-going scans thus obtained are shown in Figure 6a. The DEMS setup described earlier can be used to obtain a measure of the total Faradaic charge of $HCOO^-$ oxidation (Q_{tot}) through the primary and the secondary pathways from the mass spectrometric charge as described below.

The mass spectrometric current (I_{MS}) or the corresponding charge (Q_{MS}) obtained by integration would be linearly proportional to the Faradaic current (I_F) or the Faradaic charge (in our case, Q_{tot}) of $HCOO^-$ oxidation (eqns. 1 and 2). In eqns. 1 and 2, n is the number of electrons involved in the oxidation of $HCOO^-$ (n = 2, in this case) and K^*_{44} is a calibration constant.

$$I_F = nI_{MS}/K^*(44) \quad (1)$$

$$Q_{tot} = nQ_{MS}/K^*(44) \quad (2)$$

Q_{tot}, thus obtained, at a given time t_{hold}, is normalized to the total charge at t_{hold} = 5 s to give the normalized total Faradaic charge, Q^*_{tot}. The plot of Q^*_{tot} vs t_{hold} is shown in Figure 6b. The peak currents for the first (**Peak 1**) and the second (**Peak 2**) anodic peaks vs t_{hold} are also plotted (Figure 6b).

The Pt surface is gradually deactivated by CO_{ads} as shown by the overall decrease in the oxidation charge (Q^*_{tot}) with time (Figure 6b). It is seen that substantial CO_{ads} formation occurs only at longer times on the order of minutes. As seen from the Q^*_{tot} vs t_{hold} plot (Figure 6b), CO_{ads} formation approaches a saturation value only at times longer than 20 min. Under similar conditions of potential and concentration, a saturation coverage of CO_{ads} from HCOOH is achieved in 10 s.[3,60,61] It is amply clear that CO_{ads} formation from $HCOO^-$ is quite slow vis-à-vis HCOOH.

The coupled behavior of **Peak 1** and **Peak 2** in the positive-going scans is apparent from Figure 6. As t_{hold} increases, **Peak 1** decreases and **Peak 2** increases and an isopotential point is obtained at ~0.6 V between **Peak 1** and **Peak 2**. This is also apparent from Figure 5b, where the isopotential point, again at ~0.6 V, is clearly seen. Typically, an isopotential point is seen when there are two adsorbed species such that their total area of coverage remains constant at all times.[64] In the context of the experiment, this would imply the presence of an adsorbate whose coverage is linearly dependent on the coverage of CO_{ads}. We suspect that the adsorbate involved is the active intermediate in the primary pathway. This possibility is explored further in the adsorbate stripping experiments.

To study the potential dependence of CO_{ads} formation from $HCOO^-$, the previous potential step-scan procedure (inset to Figure 6) was modified to allow sufficient time for CO_{ads} formation. The potential program applied is shown in the inset of Figure 7a. From an initial potential of 1.3 V, the potential was stepped to a potential, E_{low} in the H_{upd} region and held for 10 min (t_{hold}) to allow sufficient time for CO_{ads} formation and then scanned anodically at 50 mV/s to 1.3 V. This procedure was repeated for different values of E_{low} ranging from 0.05 to 0.35 V vs RHE. Some representative positive-going sweeps obtained by this procedure are shown in Figure 7a. The variation of the peak currents, j^1_{peak} and j^2_{peak}, for the first (**Peak 1**) and the second peaks (**Peak 2**), respectively, in the positive-going scans with E_{low} are also plotted (Figure 7b). We see that the maximum CO_{ads} formation occurs over the potential range from 0.15 to 0.2 V. Such a maximum for CO_{ads} formation from

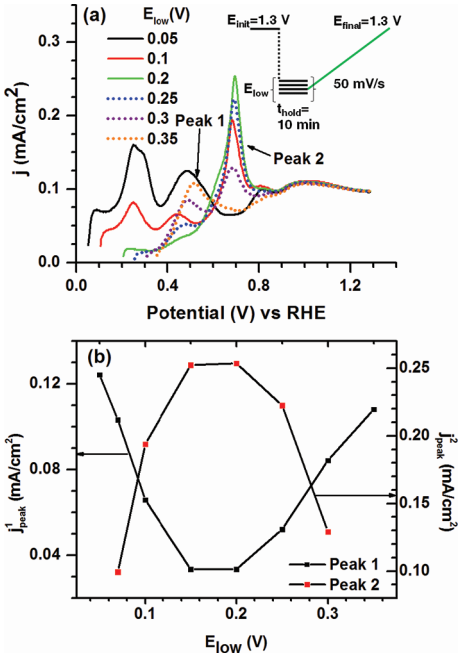

Figure 7. (a) Positive-going scans obtained after the potential step procedure shown in the inset was carried out in 0.1 M HCOONa + 0.9 M NaOH on a polycrystalline Pt disk for different values of E_{low}. Scan rate 50 mV/s (b) Plot of the first (j^1_{peak}) and the second (j^2_{peak}) peak current density versus E_{low}.

HCOOH has also been reported.[63] This has been attributed to a surface reaction, following Langmuir–Hinshelwood kinetics, which involves the reduction of either the reactive intermediate Pt-COOH[3,9] or $HCOOH_{ads}$[14] by H_{ads}. An analogous mechanism could be active in the case of $HCOO^-$. It is also to be noted that, although OH adsorption could inhibit $HCOO^-$ adsorption, the effect of the former should be negligible over the potential range (0.05–0.35 V) studied. Interestingly, **Peak 1** shows a trend opposite to that of **Peak 2** (Figure 7b) with the peak current (j^1_{peak}) going through a minimum over the same potential range (0.15–0.2 V). This is further evidence for the strong correlation between the primary and the secondary pathways. Since $HCOO^-$ would not be able to displace the strongly bound CO_{ads}, the number of sites available for $HCOO^-$ adsorption and/or formation of the active intermediate in the primary pathway should be partly dictated by the coverage of CO_{ads}. This could explain the reciprocal relationship between **Peak 1** and **Peak 2**.

3.3. Adsorbate Stripping Experiments. Since it has been shown that the oxidation of $HCOO^-$ is highly adsorbate mediated, we have carried out adsorbate stripping experiments using the flow cell described earlier. These experiments allow us to look at just the contribution of adsorbates to the electrochemical response in the absence of the solution species. In the present case, this technique allows us to look at the activity of $HCOO_{ads}$ and/or its adsorbed derivatives in the absence of $HCOO^-$ in solution. The use of the flow cell enables fast and convenient exchange of solutions under potential control. For the sake of comparison, the experiments were done in both acidic and basic media (i.e., HCOOH and $HCOO^-$ oxidation, respectively).

The experimental procedure followed is shown in Scheme 2a. At the start of the experiment, the working electrode is held at a potential, E_{dose} and exposed to the flow of blank solution (i.e.,

dx.doi.org/10.1021/jp211887x | J. Phys. Chem. C 2012, 116, 5810–5820

Scheme 2. (a) Potential Program Used for the Adsorbate Stripping Experiment (Results Shown in Figure 8a,b) Using the Flow Cell; (b) Modified Potential Program for the Adsorbate Stripping Experiment (Results Shown in Figure 8c)[a]

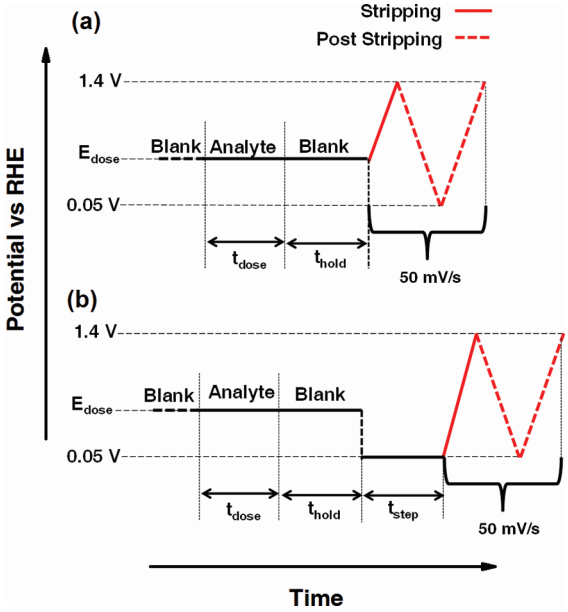

[a]Solution flow rate is 100 μL/s.

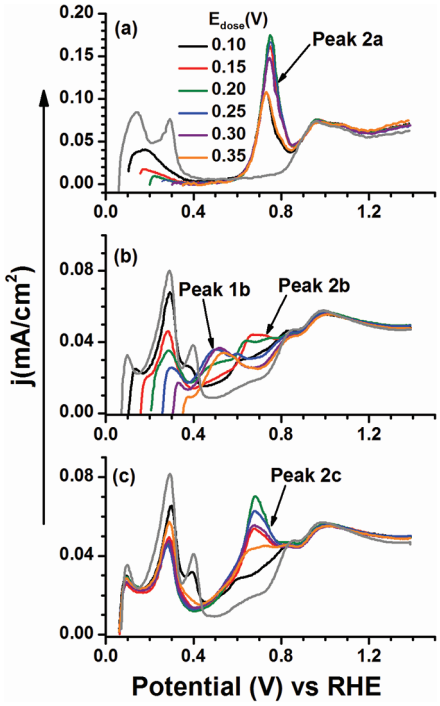

Figure 8. Stripping scans at 50 mV/s obtained at a polycrystalline Pt disk for different values of E_{dose} following (a) Scheme 2a. Analyte solution: 0.2 M HCOOH in 0.1 M H_2SO_4, Blank solution: 0.1 M H_2SO_4. t_{dose}: 5 s. t_{hold}: 120 s. (b) Scheme 2a. Analyte solution: 0.2 M HCOONa in 1 M NaOH, Blank solution: 1 M NaOH. t_{dose}: 10 s. t_{hold}: 50 s. (c) Scheme 2b. Analyte solution: 0.2 M HCOONa in 1 M NaOH, Blank solution: 1 M NaOH. t_{dose}: 10 s. t_{hold}: 50 s. t_{step}: 50 s. Post stripping scans at 50 mV/s shown in gray. The legend for part a is applicable for parts b and c.

either 1 M $HClO_4$ or 1 M NaOH). Under potential control, the flow is then switched to the analyte solution (200 mM HCOOH in 1 M $HClO_4$ or 200 mM HCOONa in 1 M NaOH) for time t_{dose}. Still maintaining potential control, at the end of time t_{dose}, the flow is switched back to the blank solution and the cell flushed with blank solution for time t_{hold}. Subsequently, a positive-going stripping scan is started from E_{dose} at 50 mV/s to the upper limit (1.4 V). A post stripping scan from 0.05 to 1.4 V was also performed to verify the absence of any electroactive adsorbates subsequent to stripping. A constant flow rate of 100 μL/s was maintained throughout. t_{dose} was 5 and 10 s in acid and in base, respectively. The dosing potentials (E_{dose}) were sampled in the H_{upd} region. The t_{hold} was 120 and 50 s in acid and in base, respectively. The results from these experiments are shown in the form of the stripping scans and the poststripping scans for both the acidic (Figure 8a) and the basic (Figure 8b) media.

In the case of acidic media (Figure 8a), we observe only one stripping peak (**Peak 2a**) at ~0.7 V which is the oxidation of CO_{ads}. No other stable adsorbate was detected. It is generally accepted that the reactive intermediate (Pt-COOH) in the direct pathway, once formed, is highly unstable immediately converting to the final oxidation product, CO_2.[9,13] On plotting the peak current ($\mathbf{j_{peak}}$) for CO_{ads} stripping peak (**Peak 2a**) vs E_{dose}, a maximum in CO_{ads} formation is observed at 0.2 V (Figure 9a). A similar volcano-type curve was observed by Sun and Yang et al. for the variation of the average rate of dissociative adsorption of HCOOH versus electrode potential for single crystal platinum electrodes.[63] Such results support the hypothesis that, at low potentials, H_{ads} is actively involved in the formation of CO_{ads}.[3,9,14]

The adsorbate stripping scans for $HCOO^-$ show two broad peaks centered at ~0.5 V (**Peak 1b**) and ~0.65 V (**Peak 2b**). Note that the potentials at which these stripping peaks occur match those of the first and the second peaks, respectively, in the positive-going scans in the presence of solution $HCOO^-$. This is further evidence that $HCOO^-$ oxidation is strongly mediated by adsorbates. We call the adsorbates, corresponding to **Peak 1b** and **Peak 2b**, **X1** and **X2**, respectively. Ostensibly, **X2** is CO_{ads}. Due to the overlap of the peaks, estimation of the charges associated with each is difficult. To help follow the trends with E_{dose}, the peak currents (j_{peak}) associated with each are plotted against E_{dose} in Figure 9b. It is seen that **Peak 2b** grows with an increase in E_{dose}, reaches a maximum at ~0.15 V and then decreases with further increases in E_{dose}. This variation of **Peak 2b** with E_{dose} is similar to the result obtained from the related experiment (Figure 7) with $HCOO^-$ in solution. At higher values of E_{dose} (>0.25 V), **Peak 2b** merges into **Peak 1b**. **Peak 1b** is visibly present only at E_{dose} > 0.2 V. It slightly increases with an increase in E_{dose}, reaches a maximum at ~0.3 V and then decreases.

The above-mentioned trends apart, the presence of **Peak 1b** is significant. It immediately suggests that $HCOO^-$ forms a stable electroactive adsorbate, **X1**, other than CO_{ads}. There are two possibilities as far as the identity of **X1** is concerned. It could be either $HCOO_{ads}$ or the active intermediate involved in the primary pathway. Of course, $HCOO_{ads}$ could also be the active intermediate.

In order to further understand the nature of the adsorbate, **X1**, a variation of the previous stripping experiment was carried out as per Scheme 2b. It follows the same procedure as Scheme 2a, except that after holding the working electrode at potential E_{dose} for time t_{hold}, the potential was stepped to 0.05 V and held

dx.doi.org/10.1021/jp211887x | J. Phys. Chem. C 2012, 116, 5810–5820

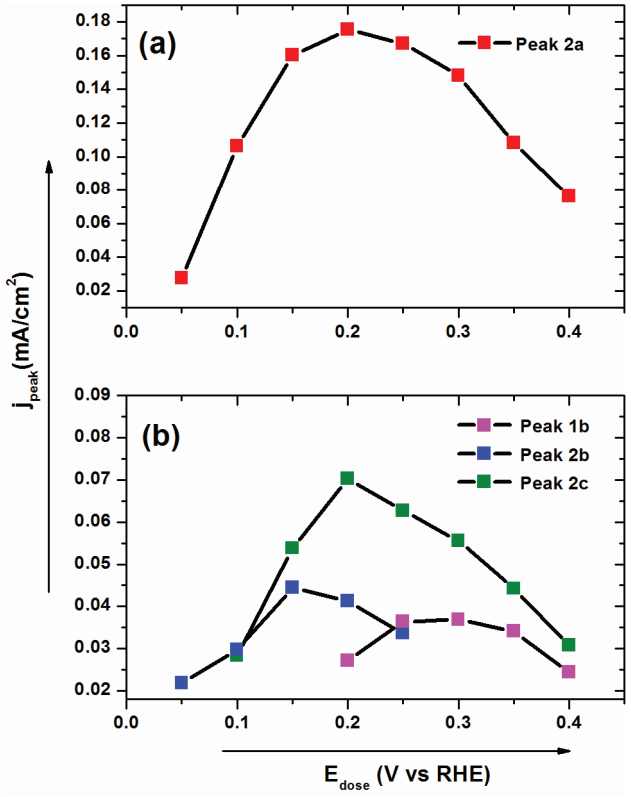

Figure 9. Plot of the peak current densities (j_{peak}) versus E_{dose} for the stripping peaks from (a) Figure 8a based in Scheme 2a (b) Figure 8b based in Scheme 2a and Figure 8c based in Scheme 2b.

for time t_{step} = 50 s. The stripping scan was then initiated from 0.05 V. As in the previous experiment, a constant flow rate of 100 μL/s was maintained throughout the duration of the potential program. The motivation for this experiment was to determine whether **X1** is weakly adsorbed or not. The rationale for the potential step to 0.05 V, after the initial adsorption of **X1** at a higher potential (E_{dose}), was that, at such a low potential in the H_{upd} region, H_{ads} would displace any weakly bound adsorbates. This would be the case for adsorption of anions such as $HCOO^-$. Consequently, we should expect **Peak 1b** to be absent in the subsequent stripping scan, if **X1** is only weakly bound. Since CO_{ads} is strongly bound, **Peak 2b** should not change significantly by this procedure.

The stripping scans from the modified stripping experiment (Scheme 2b) are shown in Figure 8c. **Peak 1b** was absent from the stripping scans. However, contrary to our expectations, **Peak 2b** was also significantly enhanced. In the interest of clarity, the stripping peak obtained by the modified procedure is called **Peak 2c**. If we attribute **Peak 2b** and **Peak 2c** mainly to CO_{ads} oxidation, then the increase in charge under **Peak 2c** compared to **Peak 2b** would mean that additional CO_{ads} is formed on stepping to low potential. This CO_{ads} has to originate from **X1** since the increase in charge under **Peak 2c** is accompanied by the disappearance of **Peak 1b**. At the same time, the latter phenomenon also shows that **X1** is not weakly adsorbed. This is so since if **X1** has to be converted to CO_{ads}, **X1** would have to be present at 0.05 V; meaning **X1** is not displaced by H_{ads}. In view of these results, $HCOO_{ads}$ seems to be an unlikely candidate for **X1**. The implication that **X1** can be converted to CO_{ads} (**X2**) directly addresses the strong correlation observed between **Peak 1** and **Peak 2** in the potential step-scan experiments (Figures 6 and 7). It is also interesting to note that the plot of the peak current ($\mathbf{j_{peak}}$) vs $\mathbf{E_{dose}}$ obtained for **Peak 2c** following the modified procedure (Scheme 2b) clearly shows a volcano type behavior with a maximum at $E_{dose} \approx 0.2$ V, similar to the case of CO_{ads} stripping from HCOOH (Figure 9a).

It would be insightful to accurately determine and compare the total adsorbate oxidation charges from the stripping scans following Scheme 2a and 2b. Accurate determination of these charges is precluded in the current case due to the overlap of the H-desorption peaks with the oxidation peaks of **X1** and **X2**. However, in an attempt to discern the trends, Faradaic charges, $\mathbf{Q_a}$ and $\mathbf{Q_b}$, were obtained by integration of the Faradaic currents in the stripping scans following Scheme 2a,b, respectively. The integration was carried out from 0.38 to 0.83 V, after background subtraction, for different values of E_{dose}. The lower limit of integration was chosen so as to mitigate the complications associated with estimation of H-desorption charges in the poststripping scan that is used for background subtraction.

Plots of $\mathbf{Q_a}$ and $\mathbf{Q_b}$ vs E_{dose} are shown in Figure 10. $\mathbf{Q_a}$ and $\mathbf{Q_b}$ vary in a similar fashion with E_{dose}; both showing a maximum at $E_{dose} \approx 0.2$ V. It is also noted that $\mathbf{Q_b}$ is higher than $\mathbf{Q_a}$ irrespective of E_{dose}. This supports the argument that **X1** is strongly adsorbed since $\mathbf{Q_b}$ should have been significantly less than $\mathbf{Q_a}$ if **X1** were desorbed in the H_{upd} region. $\mathbf{Q_b}$ would be greater than $\mathbf{Q_a}$ if the number of electrons (n) needed to oxidize **X1** is less than that of **X2**. If we assume **X2** to be CO_{ads} and the corresponding n to be 2, then it would imply that n = 1 for **X1**. However, to verify this hypothesis, a quantitative determination of the oxidation charges associated with **X1** and **X2** is needed. This is so since $\mathbf{Q_a}$ and $\mathbf{Q_b}$ do not account for the oxidation charges of **X1** and **X2** from 0.2 to 0.38 V. We are currently working on addressing this issue by a DEMS study using a modified flow cell design suitable for mass spectrometric detection of CO_2 in alkaline media.[65]

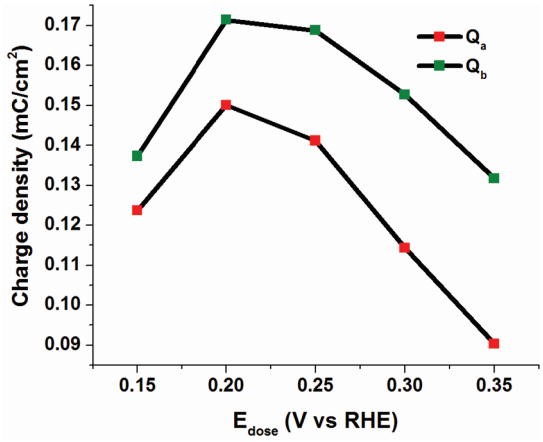

Figure 10. Plot of the charges $\mathbf{Q_a}$ and $\mathbf{Q_b}$ vs E_{dose} obtained by integration of Faradaic currents in the stripping scans following Scheme 2a (Figure 8b) and 2b (Figure 8c), respectively. Integration is carried out from 0.38 to 0.83 V after background subtraction.

4. DISCUSSION

In understanding $HCOO^-$ oxidation, it is crucial to gain some insight into the identity and nature of **X1**. As of now, **X1** appears to be a strongly adsorbed species that could be either

dx.doi.org/10.1021/jp211887x | J. Phys. Chem. C 2012, 116, 5810–5820

oxidized to CO_2 or converted to **X2** (CO_{ads}). Mechanistically, it seems reasonable to propose an oxygen-rich species with a strong Pt−C bond. The latter feature would be able to account for the strong adsorption of **X1**. Pt-COOH or an active complex of the form [Pt−CO....Pt−OH] could be two possible candidates. At this point, it is clear that in-depth spectroscopic studies are needed to unambiguously identify the chemical nature of **X1** and such work is planned in the near future.

The results so far indicate that a dual pathway mechanism is active for $HCOO^-$ oxidation. A tentative mechanism is outlined in Scheme 3. We believe that **X1** is the precursor adsorbate for

Scheme 3. Proposed Mechanism for $HCOO^-$ Oxidation

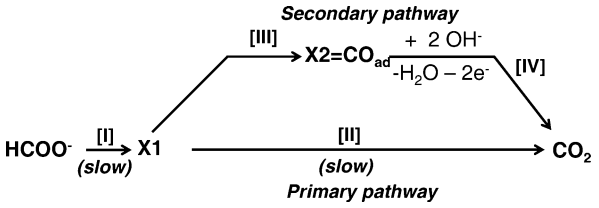

both the primary and the secondary pathways of $HCOO^-$ oxidation. It could either be oxidized to CO_2 (the primary pathway, reaction [II]) or converted to CO_{ads} (reaction [III]). CO_{ads}, thus formed, is oxidized (reaction [IV]) at higher potentials to CO_2 (the secondary pathway). Furthermore, it is indicated that both the formation of **X1** from $HCOO^-$ (reaction [I]) and the subsequent oxidation of **X1** (reaction [II]) by the primary pathway are kinetically slow. This is in contrast to the direct pathway in HCOOH oxidation, where formation of the reactive intermediate (Pt-COOH) and its subsequent oxidation are fast electrochemical steps.[9] Since we detect CO_{ads} formation from $HCOO^-$ at potentials <0.2 V, we note the possibility that CO_{ads} can be formed from $HCOO^-$ or $HCOO_{ads}$. However, it is not clear whether **X1** is an intermediate in this reaction.

On the basis of the proposed mechanism, we attempt to explain some of the features of $HCOO^-$ oxidation. The overall low activity of $HCOO^-$ vis-à-vis HCOOH can be attributed to the slow kinetics of formation and oxidation of **X1** (reaction [I] and [II] respectively). Since no oxidation occurs in the negative-going scan above ∼0.7 V (Figure 2), formation of **X1** is likely inhibited by Pt-oxide. It could also be that $HCOO^-$ transitions from an electroactive species to a spectator anion at potentials positive of PZC.[54−56] It was also seen that CO_{ads} formation from $HCOO^-$ was quite slow (Figure 6) vis-à-vis HCOOH in acid. Further, under potential cycling conditions, it was seen (Figure 2 and 3) that **Peak 2** in the positive-going scan (mainly CO_{ads} oxidation) is always smaller than **Peak 1** (mainly primary pathway). The slow kinetics of CO_{ads} formation is explained as follows. In the case of HCOOH, CO_{ads} can be formed from the reactive intermediate (Pt-COOH) or independently by spontaneous dissociative adsorption of HCOOH.[9] However, in the case of $HCOO^-$, formation of CO_{ads} is controlled primarily by the formation (reaction [I]) and subsequent conversion (reaction [III]) of **X1**. Since the formation of **X1** (reaction [I]) is kinetically limited, CO_{ads} formation would also be slow. It was also seen that a decrease in CO_{ads} formation did not appreciably enhance the oxidation of $HCOO^-$ through the primary pathway (Figure 5). This is so since the rate-limiting steps in the oxidation of $HCOO^-$ would be the reactions associated with **X1** (reactions [I] and [II]) and not the oxidation of CO_{ads}. Another interesting feature of the $HCOO^-$ oxidation was the strongly correlated behavior of **Peak 1** and **Peak 2** in the positive-going scans as seen in the potential step-scan experiments (Figures 6 and 7). We attribute this to the partitioning of **X1** between the primary and the secondary pathways.

It is important to consider the effects of OH adsorption on $HCOO^-$ oxidation. As has already been noted, under potential cycling conditions, we observe that the oxidation currents in the negative-going scans are generally smaller than those in the positive-going scans. We attributed this to blocking of surface sites for $HCOO^-$ adsorption by OH_{ads} in the negative-going scan. Thus, OH adsorption can add to the kinetic complications in the formation of **X1** (reaction [I]). However, due to the presence of OH_{ads} at low potentials, the oxidation of CO_{ads} (reaction [IV]) is quite early at ∼0.35 V vs RHE (see Figure 6).

5. CONCLUSIONS

These studies show that oxidation of $HCOO^-$ in alkaline medium happens to a significantly lower extent when compared to HCOOH in acidic medium. A dual pathway mechanism (Scheme 3), analogous to HCOOH oxidation, seems to be applicable for $HCOO^-$ oxidation. From combined cyclic voltammetric-DEMS studies, it was found that the activity of $HCOO^-$ is confined to the potential range ∼0.2−0.7 V vs RHE. Also, formation of the active intermediate in $HCOO^-$ oxidation is indicated to be adversely affected by OH adsorption. Potential step-scan expereiments revealed CO_{ads} formation from $HCOO^-$ to be slow. Moreover, it is observed that the primary and the secondary pathways of $HCOO^-$ oxidation are strongly correlated. Adsorbate stripping experiments showed the presence of a stable adsorbate, **X1** in addition to CO_{ads}. **X1** is shown to undergo oxidation in the same potential range in which the primary pathway is active. Additionally, **X1** can be converted to CO_{ads} in the presence of H_{ads}. Further studies are planned to identify the nature of this adsorbate. On the basis of the results obtained, a tentative mechanism is proposed. According to this mechanism, $HCOO^-$ oxidation is mediated exclusively by the formation of **X1**, which is thought to serve as the precursor adsorbate for both the primary and the secondary pathways of $HCOO^-$ oxidation.

AUTHOR INFORMATION

Corresponding Author

*Tel.: (607) 255-4720; fax: (607) 255-9864; e-mail: hda1@cornell.edu.

ACKNOWLEDGMENTS

This material is based upon work supported as part of the Energy Materials Center at Cornell (EMC2), an Energy Frontier Research Center funded by the U.S. Department of Energy, Office of Science, Office of Basic Energy Sciences under Award No. DE-SC0001086. J.J. would like to thank IPMI and Gemini Industries for the 2011 IPMI Gemini graduate student award.

REFERENCES

(1) Capon, A.; Parson, R. *J. Electroanal. Chem. Interfacial Electrochem.* **1973**, *44*, 1−7.

(2) Capon, A.; Parsons, R. *J. Electroanal. Chem. Interfacial Electrochem.* **1973**, *44*, 239−254.

(3) Capon, A.; Parsons, R. *J. Electroanal. Chem. Interfacial Electrochem.* **1973**, *45*, 205−231.
(4) Clavilier, J.; Parsons, R.; Durand, R.; Lamy, C.; Leger, J. M. *J. Electroanal. Chem.* **1981**, *124*, 321−326.
(5) Beden, B.; Bewick, A.; Lamy, C. *J. Electroanal. Chem. Interfacial Electrochem.* **1983**, *148*, 147−160.
(6) Kunimatsu, K. *J. Electroanal. Chem. Interfacial Electrochem.* **1986**, *213*, 149−157.
(7) Kunimatsu, K.; Kita, H. *J. Electroanal. Chem. Interfacial Electrochem.* **1987**, *218*, 155−172.
(8) Corrigan, D. S.; Weaver, M. J. *J. Electroanal. Chem. Interfacial Electrochem.* **1988**, *241*, 143−162.
(9) Sun, S. G.; Clavilier, J.; Bewick, A. *J. Electroanal. Chem. Interfacial Electrochem.* **1988**, *240*, 147−159.
(10) Parsons, R.; VanderNoot, T. *J. Electroanal. Chem. Interfacial Electrochem.* **1988**, *257*, 9−45.
(11) Leung, L. W. H.; Weaver, M. J. *Langmuir* **1990**, *6*, 323−333.
(12) Iwasita, T.; Nart, F. C.; Lopez, B.; Vielstich, W. *Electrochim. Acta* **1992**, *37*, 2361−2367.
(13) Lu, G.-qiang; Crown, A.; Wieckowski, A. *J. Phys. Chem. B* **1999**, *103*, 9700−9711.
(14) Wieckowski, A.; Sobkowski, J. *J. Electroanal. Chem. Interfacial Electrochem.* **1975**, *63*, 365−377.
(15) Miki, A.; Ye, S.; Osawa, M. *Chem. Commun.* **2002**, 1500−1501.
(16) Samjeské, G.; Osawa, M. *Angew. Chem. (Int. Ed. Engl.)* **2005**, *44*, 5694−5698.
(17) Samjeské, G.; Miki, A.; Ye, S.; Yamakata, A.; Mukouyama, Y.; Okamoto, H.; Osawa, M. *J. Phys. Chem. B* **2005**, *109*, 23509−23516.
(18) Samjeské, G.; Miki, A.; Ye, S.; Osawa, M. *J. Phys. Chem. B* **2006**, *110*, 16559−16566.
(19) Osawa, M.; Komatsu, K.-I.; Samjeské, G.; Uchida, T.; Ikeshoji, T.; Cuesta, A.; Gutiérrez, C. *Angew. Chem. (Int. Ed. Engl.)* **2011**, *50*, 1159−63.
(20) McLean, G. *Int. J. Hydrogen Energy* **2002**, *27*, 507−526.
(21) Varcoe, J. R.; Slade, R. C. T. *Fuel Cells* **2005**, *5*, 187−200.
(22) Prabhuram, J.; Manoharan, R. *J. Power Sources* **1998**, *74*, 54−61.
(23) Spendelow, J. S.; Wieckowski, A. *Physical Chem. Chem. Phys.* **2007**, *9*, 2654−2675.
(24) Lamy, C.; Belgsir, E. M.; Léger, J.-M. *J. Appl. Electrochem.* **2001**, *31*, 799−809.
(25) Tripković, A. V.; Popović, K. D.; Grgur, B. N.; Blizanac, B.; Ross, P. N.; Marković, N. M. *Electrochim. Acta* **2002**, *47*, 3707−3714.
(26) Hao, Yu; E. Scott, K.; Reeve, R. W. *J. Electroanal. Chem.* **2003**, *547*, 17−24.
(27) Christensen, P. A.; Linares-Moya, D. *J. Phys. Chem. C* **2010**, *114*, 1094−1101.
(28) Buck, R. P.; Griffith, L. R. *J. Electrochem. Soc.* **1962**, *109*, 1005.
(29) Conway, B. E.; Dzieciuch, M. *Can. J. Chem.* **1963**, *41*, 38−54.
(30) Günther, H.; Wetzel, R.; Müller, L. *Electrochim. Acta* **1979**, *24*, 237−238.
(31) Wetzel, R.; Günther, H.; Müller, L. *J. Electroanal. Chem. Interfacial Electrochem.* **1979**, *103*, 271−275.
(32) Beden, B.; Lamy, C.; Leger, J. M. *J. Electroanal. Chem. Interfacial Electrochem.* **1979**, *101*, 127−131.
(33) Adžić, R. R.; Hofman, M. I.; Dražić, D. M. *J. Electroanal. Chem. Interfacial Electrochem.* **1980**, *110*, 361−368.
(34) Christensen, P. A.; Hamnett, A.; Linares-Moya, D. *Phys. Chem. Chem. Phys.* **2011**, *13*, 11739−11747.
(35) Baltruschat, H. *J. Am. Soc. Mass Spectrom.* **2004**, *15*, 1693−706.
(36) Chen, Y. X.; Heinen, M.; Jusys, Z.; Behm, R. J. *Angew. Chem. (Int. Ed. Eng.)* **2006**, *45*, 981−985.
(37) Chen, Q.-S.; Sun, S.-G.; Zhou, Z.-Y.; Chen, Y.-X.; Deng, S.-B. *Phys. Chem. Chem. Phys.* **2008**, *10*, 3645−54.
(38) Jusys, Z.; Massong, H.; Baltruschat, H. *J. Electrochem. Soc.* **1999**, *146*, 1093−1098.
(39) Wang, H.; Löffler, T.; Baltruschat, H. *J. Appl. Electrochem.* **2001**, *31*, 759−765.
(40) Baltruschat, H. In *Interfacial Electrochemistry: Theory, Experiment and Applications*; Wieckowski, A., Ed.; Marcel Dekker Inc.: New York, 1999; pp 577−597.
(41) Wang, H.; Rus, E.; Abruña, H. D. *Analytical chemistry* **2010**, *82*, 4319−24.
(42) Wang, H.; Alden, L.; Disalvo, F. J.; Abruña, H. D. *Physical chemistry chemical physics* **2008**, *10*, 3739−51.
(43) Kutschker, A.; Vielstich, W. *Electrochim. Acta* **1962**, *8*, 985−989.
(44) Kita, H.; Ye, S.; Aramata, A.; Furuya, N. *J. Electroanal. Chem. Interfacial Electrochem.* **1990**, *295*, 317−331.
(45) Marinković, N. S.; Marković, N. M.; Adžić,, R. R. *J. Electroanal. Chem.* **1992**, *330*, 433−452.
(46) Marković, N. M.; Gasteiger, H. A.; Ross, P. N. *J. Phys. Chem.* **1996**, *100*, 6715−6721.
(47) Marković, N. M.; Sarraf, S. T.; Gasteiger, H. A.; Ross, P. N. *J. Chem. Soc., Faraday Trans.* **1996**, *92*, 3719.
(48) Spendelow, J. S.; Lu, G. Q.; Kenis, P. J. A.; Wieckowski, A. *J. Electroanal. Chem.* **2004**, *568*, 215−224.
(49) Spendelow, J. S.; Goodpaster, J. D.; Kenis, P. J. A.; Wieckowski, A. *J. Phys. Chem. B* **2006**, *110*, 9545−9555.
(50) Marković, N. M.; Lucas, C. A.; Rodes, A.; Stamenković, V. R.; Ross, P. N. *Surf. Sci.* **2002**, *499*, L149−L158.
(51) García, G.; Koper, M. T. M. *Phys. Chem. Chem. Phys.* **2008**, *10*, 3802−3811.
(52) Couto, A.; Rincón, A.; Pérez, M. C.; Gutiérrez, C. *Electrochim. Acta* **2001**, *46*, 1285−1296.
(53) Munson, R. A. *J. Electrochem. Soc.* **1964**, *111*, 372.
(54) Gileadi, E.; Argade, S. D.; Bockris, J. O. *J. Phys. Chem.* **1966**, *70*, 2044−2046.
(55) Bockris, J. O.; Argade, S. D.; Gileadi, E. *Electrochim. Acta* **1969**, *14*, 1259−1283.
(56) Peretz, Y.; Yarnitzky, C. N. *J. Electroanal. Chem.* **2001**, *498*, 87−92.
(57) Vela, M. E.; Lezna, R. O.; Tacconi, N. R.; De; Arvia, A. J.; Beden, B.; Hahn, F.; Lamy, C. *J. Electroanal. Chem.* **1992**, *323*, 289−302.
(58) Miki, A.; Ye, S.; Osawa, M. *Chem. Commun.* **2002**, *2002*, 1500−1501.
(59) Neurock, M.; Janik, M.; Wieckowski, A. *Faraday Discuss.* **2009**, *140*, 363.
(60) Breiter, M. *Electrochim. Acta* **1963**, *8*, 447−456.
(61) Breiter, M. *Electrochim. Acta* **1963**, *8*, 457−470.
(62) Tripković, A. V.; Popović, K. D.; Momčilović, J. D.; Dražić, D. M. *J. Electroanal. Chem.* **1996**, *418*, 9−20.
(63) Sun, S.-g.; Yang, Y.-y. *J. Electroanal. Chem.* **1999**, *467*, 121−131.
(64) Untereker, D. F.; Bruckenstein, S. *Anal. Chem.* **1972**, *44*, 1009−1020.
(65) Bayer, D.; Cremers, C.; Baltruschat, H.; Tübke, J. *ECS Trans.* **2010**, *25*, 85−93.